Greenland Ice Sheet Surface Mass Balance Variability (1988–2004) from Calibrated Polar MM5 Output*

JASON E. BOX,[+] DAVID H. BROMWICH,[+] BRUCE A. VEENHUIS,[+] LE-SHENG BAI,[#] JULIENNE C. STROEVE,[@] JEFFREY C. ROGERS,[&] KONRAD STEFFEN,[**] T. HARAN,[@] AND SHENG-HUNG WANG[#]

[+] *Polar Meteorology Group, Byrd Polar Research Center, and Atmospheric Sciences Program, Department of Geography, The Ohio State University, Columbus, Ohio*

[#] *Polar Meteorology Group, Byrd Polar Research Center, The Ohio State University, Columbus, Ohio*

[@] *National Snow and Ice Data Center, University of Colorado, Boulder, Colorado*

[&] *Atmospheric Sciences Program, Department of Geography, The Ohio State University, Columbus, Ohio*

[**] *Cooperative Institute for Research in Environmental Sciences, University of Colorado, Boulder, Colorado*

(Manuscript received 9 May 2005, in final form 29 September 2005)

ABSTRACT

Regional climate model runs using the fifth-generation Pennsylvania State University–National Center for Atmospheric Research Mesocale Model modified for use in polar regions (Polar MM5), calibrated by independent in situ observations, demonstrate coherent regional patterns of Greenland ice sheet surface mass balance (SMB) change over a 17-yr period characterized by warming (1988–2004). Both accumulation and melt rates increased, partly counteracting each other for an overall negligible SMB trend. However, a 30% increase in meltwater runoff over this period suggests that the overall ice sheet mass balance has been increasingly negative, given observed meltwater-induced flow acceleration. SMB temporal variability of the whole ice sheet is best represented by ablation zone variability, suggesting that increased melting dominates over increased accumulation in a warming scenario. The melt season grew in duration over nearly the entire ablation zone by up to 40 days, 10 days on average. Accumulation area ratio decreased by 3%. Albedo reductions are apparent in five years of the Moderate Resolution Imaging Spectroradiometer (MODIS) derived data (2000–04). The Advanced Very High Resolution Radiometer (AVHRR)-derived albedo changes (1988–99) were less consistent spatially. A conservative assumption as to glacier discharge and basal melting suggests an ice sheet mass loss over this period greater than 100 $km^3\ yr^{-1}$, framing the Greenland ice sheet as the largest single glacial contributor to recent global sea level rise. Surface mass balance uncertainty, quantified from residual random error between model and independent observations, suggests two things: 1) changes smaller than approximately 200 $km^3\ yr^{-1}$ would not satisfy conservative statistical significance thresholds (i.e., two standard deviations) and 2) although natural variability and model uncertainty were separated in this analysis, the magnitude of each were roughly equivalent. Therefore, improvements in model accuracy and analysis of longer periods (assuming larger changes) are both needed for definitive mass balance change assessments.

1. Introduction

Ice sheet mass balance fluctuations influence global sea level and the ocean thermohaline circulation. However, the uncertainty of ice sheet mass balance components remains high (van der Veen 2002) and error bars have largely been based either on differences among estimates (Church et al. 2001) or natural variability (Hanna et al. 2005). Greenland ice sheet surface mass balance components have been resolved by statistical compilations of available observational data (e.g., Ohmura et al. 1999; McConnell et al. 2001; Cogley 2004). However, these lack either the temporal dimension or complete spatial coverage.

Recently, high-resolution limited-area regional climate models (RCMs) have been applied to fill this space–time gap over the Greenland ice sheet and investigate the spatial and temporal variability of surface mass balance components (e.g., Bromwich et al. 2001a,b; Cassano et al. 2001; Dethloff et al. 2002; Box

* Byrd Polar Research Center Contribution Number 1319.

Corresponding author address: Jason E. Box, Byrd Polar Research Center, The Ohio State University, 1090 Carmack Rd., Columbus, OH 43210-1002.
E-mail: box.11@osu.edu

and Rinke 2003; Box et al. 2004). Similarly, Hanna et al. (2002, 2005) have used global mesoscale reanalysis products to represent regional climate variability over the Greenland ice sheet. Kiilsholm et al. (2003) employ the High-Resolution Limited Area Model (HIRLAM), which includes the European Centre Hamburg Model version 4 (ECHAM4) physical parameterizations over Greenland to predict increases in melt and accumulation in a likely future greenhouse warming scenario. Horizontal grid spacing remains a challenge for RCMs in resolving the ablation zone, which ranges from less than 1 km to roughly 150 km in width. Thus, various downscaling techniques have been applied in GCMs (Wild et al. 2003) and RCMs (e.g., Box et al. 2004; Hanna et al. 2005) to represent the ablation zone. RCMs are commonly configured to be driven by "analysis" datasets (i.e., model compilations of available satellite, station, and weather balloon observations). RCMs run in this mode can thus be thought of as physically based interpolators used to provide information for regions not benefiting from direct observations.

Automatic weather station (AWS) observations (Steffen et al. 1996) and glacier survey data (Greuell et al. 2001) have proven vital in assessing skill in RCM mass balance applications over the Greenland ice sheet. RCMs have proven to offer accurate representation of temporal variability (Bromwich et al. 2001a; Cassano et al. 2001; Box and Rinke 2003; Box et al. 2004). However, apparently small systematic biases, particularly in near-surface vertical temperature and wind speed gradients and radiation fluxes, can strongly bias modeled melt rates (Box et al. 2004). Rather than presume that the propagation of systematic error can be eliminated from RCM output by continual model refinement, AWS and glacier survey data facilitate elimination of systematic model output error, to deliver observationally constrained surface climatology estimates applicable in mass balance studies. Details of the validation of the fifth-generation Pennsylvania State University–National Center for Atmospheric Research (PSU–NCAR) Mesocale Model modified for use in polar regions (Polar MM5) RCM over Greenland are found in Bromwich et al. (2001a), Cassano et al. (2001), and Box et al. (2004). Additional validation work is presented here.

Recent temperature variability suggests that the early 2000s are a special time to study ice sheet mass balance. Over the past two decades, global terrestrial records (Hansen et al. 1999) and Greenland regional temperature records (Cappelen 2004) exhibit sharp increases (Fig. 1), with North Hemisphere paleoclimatic reconstructions suggesting that the past decade has been the warmest globally for at least 2000 years (Jones and Mann 2004). Greenland temperatures reached a maximum in the 1930s after which cooling prevailed until the early 1980s (Box 2002). Warming since the mid-1980s has brought once anomalously cold Greenland regional temperatures into synchroneity with the global warming pattern. Therefore, taken in context, our results should represent the Greenland ice sheet response to rapid warming.

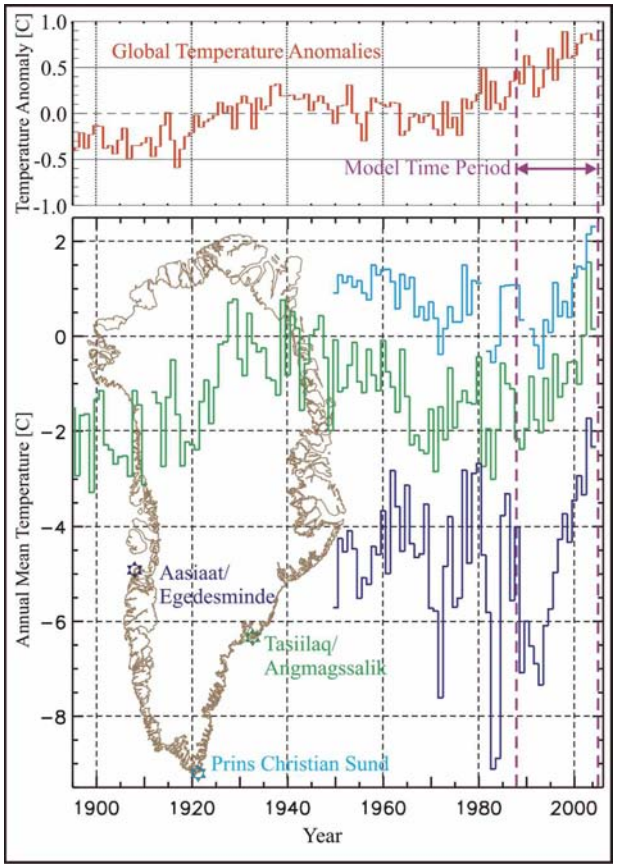

FIG. 1. (top) Global and (bottom) Greenland regional temperature records (1895–2004) and locations, including time period of model simulations in this study.

Box et al. (2004) demonstrated that summer temperature and annual precipitation variability explain >80% of the variance in 10 modeled surface mass balance years (1991–2000). Here, the temporal variability in accumulation and ablation rates is further explored, with a larger 17-yr dataset (1988–2004). Regional and overall surface mass balance variability is considered. Through this analysis, we seek to answer: Which factor *has dominated* the *overall* surface mass balance trend: *ablation or accumulation?* An answer to this question will identify Greenland's role as a future contributor to or detractor from ocean level change and its freshwater forcing in likely future scenarios of climate warming. Through model comparisons with independent obser-

vations, we provide estimates of surface mass balance uncertainty.

2. Data

Data independent of the atmospheric analyses driving the Polar MM5 model are vital in assessing errors over the Greenland ice sheet (Box et al. 2004), and these have been gathered to test and, where possible, improve the accuracy of our modeled surface mass balance results.

a. Ablation zone surface mass balance

Glacier surface mass balance is measured as the height change between the surface and a coordinate system fixed relative to the ice beneath. Surface height change is typically measured in successive end of summer (or winter) "balance years," rather than for calendar years, and are typically made along elevation profiles (e.g., Greuell et al. 2001). The fixed coordinate is usually provided by metal pipes. The metal pipes can also host instruments that sample meteorological variables and snow surface height. Such measurements along two profiles in western Greenland (separated north–south by ~260 km) are used in this study. The Institute for Marine and Atmospheric Research Utrecht (IMAU) "K-Transect" indicated in Fig. 2, e.g., Oerlemans and Vugts 1993; Greuell et al. 2001) provides 76 balance-year samples. The Program for Arctic Regional Climate Assessment (PARCA) Greenland Climate Network (GC-Net) Automatic Weather Station (AWS) in the Jakobshavn Ablation Region (JAR), Fig. 2, (Steffen et al. 1996; Steffen and Box 2001) provide 24 balance-year samples.

b. Snow pits

Snow pit density measurements at 10-cm intervals have been collected during GC-Net AWS maintenance visits. These data facilitate establishment of accumulation rates for specific summer balance years. Data from snow pits distributed widely (Fig. 2) over the GC-Net (34 balance-year samples) are available to assess errors in modeled accumulation rate.

c. Surface albedo

We incorporate two satellite-derived albedo products to define absorbed solar irradiance in modeled surface energy budget calculations. The first spans 1982–99 [i.e., the 1400 UTC 25-km Advanced Very High Resolution Radiometer (AVHRR) Polar Pathfinder "Extended" albedo data product (APP-x) (Key et al. 2002]. Different satellite platforms [e.g., the NOAA satellites (*NOAA-7, -9, -11, -14*)] were used in constructing the AVHRR time series. Although effort has gone into

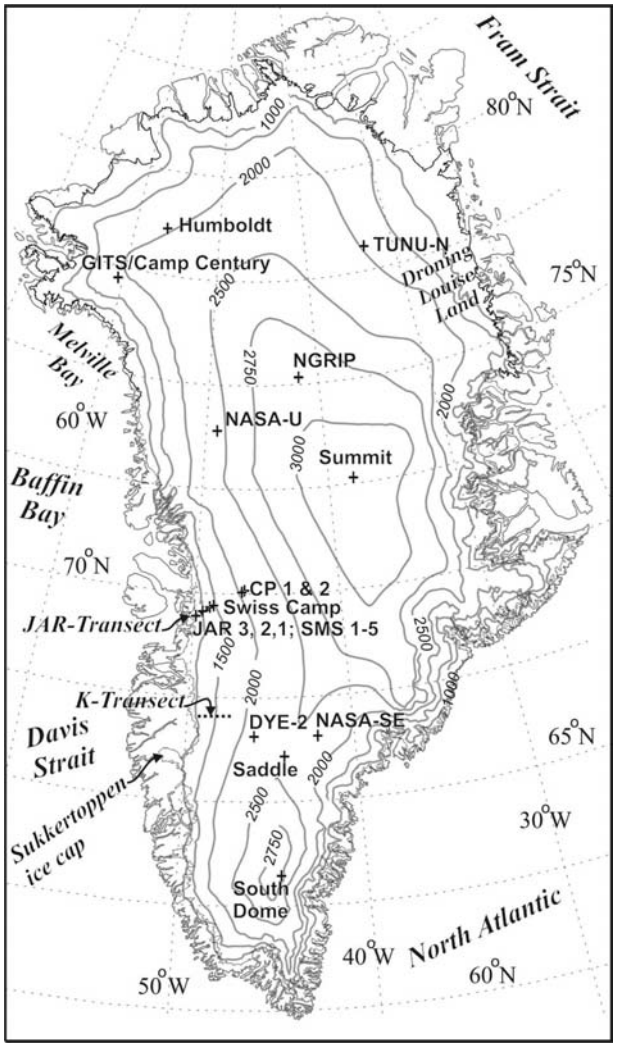

FIG. 2. Location map for surface mass balance data. Snow pits were taken at sites represented by plus signs. The ablation zone measurement transects are indicated.

removing various sources of sensor drift (Rao and Chen 1995), sensor-to-sensor inhomogeneity remains a source of uncertainty in this study. AVHRR geolocation accuracy is typically 2–3 km for the 1.25-km processing; however, geolocation errors can be as large as 10–12 km. There are other sources of geolocation error, such as spacecraft attitude variations (Baldwin and Emery 1995).

Albedo data for the 2000–04 period, when AVHRR data are currently unavailable, can be derived from a newer and potentially more accurate data product, that is, from the Moderate Resolution Imaging Spectroradiometer (MODIS). MODIS-derived albedo is based on the Liang et al. (2005) direct estimation algorithm (DEA). Intercomparison of AVHRR- and MODIS-derived albedo datasets in this study with GC-Net AWS

TABLE 1. Comparison of satellite-derived albedo with in situ observations.

Sensor	Product	Time period	No. of observations		Rms error (dimensionless)	Mean bias (dimensionless)
			Days	Years		
AVHRR	APP-x	1 Apr 1995–20 Sep 1999	4113	11.27	0.014	−0.034
MODIS	DEA	1 Apr 2000–20 Sep 2004	2861	7.84	0.007	−0.058

albedo observations reveals errors and bias (satellite minus ground observations) consistent with Stroeve et al. (2001) for AVHRR (Table 1) and with Stroeve et al. (2005) for MODIS albedo. It is noteworthy that the comparisons of Stroeve et al. (2001, 2005) were for clear-sky conditions only. We repeat the comparison using daily integrated in situ albedo (van den Broeke et al. 2004) for all-sky conditions (i.e., including both clear and cloudy conditions) and for times when solar zenith angles were less than 75°. Satellite albedo estimates are based on data from daily afternoon (12–15 h local time) snapshots. According to comparison with surface observations (Table 1), the mean MODIS albedo bias appears to be significant (i.e., the bias being larger than the rms error). We subtract the respective mean bias values from the MODIS and AVHRR albedo grids in an attempt to intercalibrate the two albedo datasets.

3. Polar MM5 surface mass balance modeling

The MM5 has been modified for use in polar regions (Bromwich et al. 2001a; Cassano et al., 2001). Polar MM5 is reinitialized once a day and continuously updated at the lateral boundaries using the twice-daily 2.5° horizontal resolution European Centre for Medium-Range Weather Forecasts (ECMWF) operational analyses. We integrate 6-hourly model output into annual distributions of surface mass balance (B) components, that is, solid and liquid precipitation (P_{solid}, P_{liquid}), surface water vapor flux (E), blowing snow sublimation (Q_S), and meltwater runoff (R). Total precipitation (P); that is, $P_{\text{solid}} + P_{\text{liquid}}$ represents large-scale (i.e., frontal and orographic) precipitation with negligible convective contributions. Here E includes upward and downward surface fluxes of water vapor from a frozen surface, that is, i.e., sublimation and deposition, and from a melting surface, that is, evaporation and condensation, respectively; E includes a model bias correction based on independent in situ data (Box et al. 2004). Accumulation rate (C) was calculated as $P - E - Q_S$. The surface mass balance B was calculated as $C - R$. Runoff is meltwater production (M) minus meltwater retention, defined using the conceptual model of Pfeffer et al. (1991). The P_{liquid} contributes directly to M. Different "facies" zones, after Benson (1962), are used in discussion: the *ablation zone*, where B is negative; the *percolation zone*, where some melting occurs but B remains positive owing to more mass accumulation by precipitation than mass loss by runoff and evaporation/sublimation; and the *dry snow zone*, where water production is essentially zero, here taken as melting less than 2 mm (w.e.), Box et al. (2004) provides more details. The present study makes additional error analyses, to better quantify uncertainty. Of note is that the model configuration was not optimized for Greenland per se; however, this study was pursued given the opportunity to extract useful information from a simulation byproduct for a higher-resolution nested model domain over Iceland (Bromwich et al. 2005). For the purposes of this study, the model was run over an additional 7 years with the configuration unchanged, providing data spanning 17 years (1988–2004). The ice sheet area in the 24-km model domain is 1.691×10^6 km^2, tuned to match the correct value using the Ekholm (1996) land–ice–ocean mask, and includes 2936 grid cells of 576 km^2 area.

4. Model error assessment and control

We incorporate independent observational data to assess Polar MM5 surface mass balance errors. Furthermore, for cases where there is a systematic bias and a reasonably high spatial/temporal correlation exists between modeled and observed surface mass balance, the independent validation data can be used (beyond error assessment) to remove systematic biases via statistical regression. Once all statistically explained variance is removed, the residual (apparently random) error is useful to quantify overall uncertainty. Residual errors are attributable to the combination of inadequate model physical parameterizations and observational errors. Sources of Polar MM5 model "state variable" errors, for example, temperature, humidity, wind speed, and pressure, are discussed in Bromwich et al. (2001a) and BLBBS. Cassano et al. (2001) and Box et al. (2004) discuss state-variable errors and errors related to the surface energy budget. Despite reasonably high correlations (e.g., greater than 0.9 for temperature), systematic biases (gradients and offsets) also exist in Polar MM5 surface air (at 2 m) and ground temperatures, wind speed, and radiation fluxes, which amplify residual melt energy used to derive meltwater production

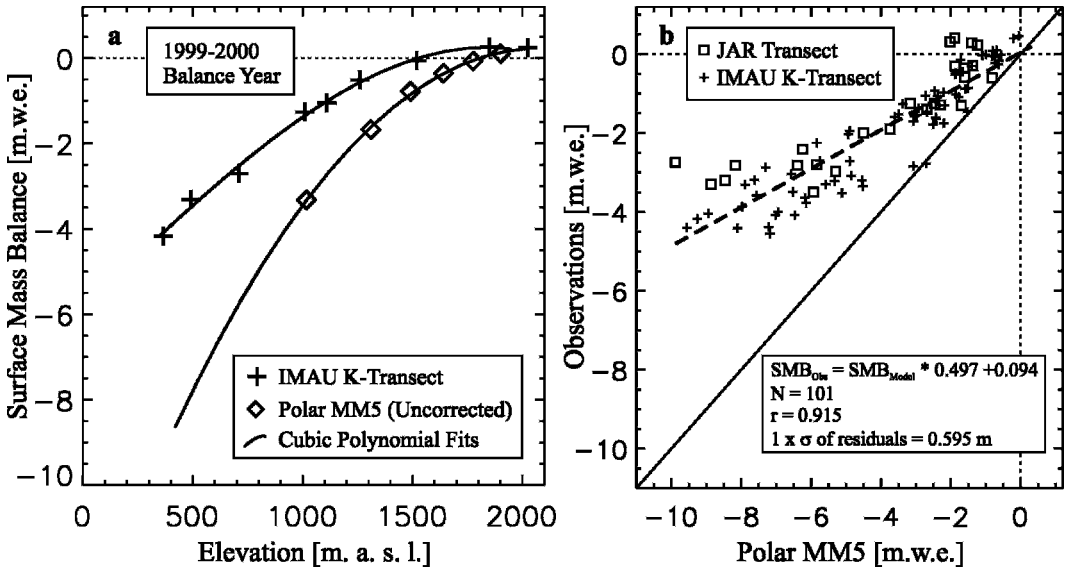

FIG. 3. (a) Example of a single observed and modeled balance-year profile (1999–2000) along the IMAU K-transect. (b) Comparison between modeled surface mass balance interpolated to observational sites at K-Transect and JAR transect sites, with regression fit to available data and the equation used to remove systematic bias for ablation zone sites.

(Box et al. 2004). Energy balance calculations produce a residual "melt energy" term that is converted to water equivalent depth meltwater production (m w.e. or mm w.e.), when the surface temperature has reached the melting point. If the model skill is high for basic variables, but systematic biases produce unrealistic derivatives, the modeled melt rates remain inaccurate. Here, we believe we have sufficient observational constraint from independent data to assess the model accuracy and to remove the main model biases, making the modeled surface mass balance output more reliable. The regression-based adjustments do not, however, guarantee increased accuracy everywhere in the model domain owing to spatially limited validation data. Nor does this correction guarantee equal improvement in all years. Improved model physics, higher spatial resolution, and better boundary conditions (i.e., data assimilation products) are important ways to further improve model accuracy.

5. Methods

a. Ablation zone surface mass balance

A cubic polynomial least squares statistical model is fit to modeled and observed ablation rates in terms of elevation, the latter being the "independent" variable. As such, the cubic function allows a downscaled comparison of uncorrected model surface mass balance values with observations at specific elevations (Fig. 3a). Linear regression of observed and modeled surface mass balance differences at the observation site elevations facilitates the creation of a statistical model for Polar MM5 systematic bias (Fig. 3b). This comparison represents areas at or below the equilibrium line altitude (ELA). The one standard deviation of residual error for this regression is ±0.595 m. The mean model bias is removed from all below-ELA Polar MM5 grid cells where meltwater production is registered using the same bias function illustrated in Fig. 3b. Above the ELA, only the regression slope (α_1) value is used to reduce model melt energy. This partitioning produces a 10-yr average match for surface mass balance from sites at or above the ELA, where some runoff occurs (i.e., Swiss Camp and IMAU K-transect sites 9 and 10). Table 2 lists separate regression results for the JAR and K transects. Both transects demonstrate similar model errors. A combined site correction function, illustrated in Fig. 3b, was used to correct the entire Greenland ice sheet ablation zone surface mass balance bias. The relatively high correlation coefficient suggests that this correction function captures the majority of the variance, that is, more than 80%, and is not significantly degraded by low sample population or by skewness.

b. Accumulation rates

Annual-specific accumulation rates (C) derived from snow pits distributed widely (Fig. 2) were also compared with modeled values (Fig. 4) to measure system-

TABLE 2. Statistics of regression between observed and modeled ablation zone surface mass balance for individual elevation transects.

Transect	N	25
JAR	Regression slope	0.4062
	Regression offset	0.1042
	Correlation coefficient	0.8774
	$1 \times \sigma$ of residuals	0.6152
	Skewness of residuals	0.226
K	N	76
	Regression slope	0.5354
	Regression offset	0.1046
	Correlation coefficient	0.9438
	$1 \times \sigma$ of residuals	0.508
	Skewness of residuals	−0.5865

atic and residual model uncertainty. The comparison suggests a positive bias in modeled accumulation rate, consistent with model overestimated precipitation rates at coastal stations (not shown). The Polar MM5 mean accumulation rate, corrected for the entire model domain, using the regression function illustrated in Fig. 4 is discussed in the results section 6a.

c. Integration of surface mass balance uncertainty

Surface mass balance magnitude exhibits a strong elevation dependence in glacier survey data (e.g., Greuell et al. 2001) and in Polar MM5 results (Box et al. 2004).

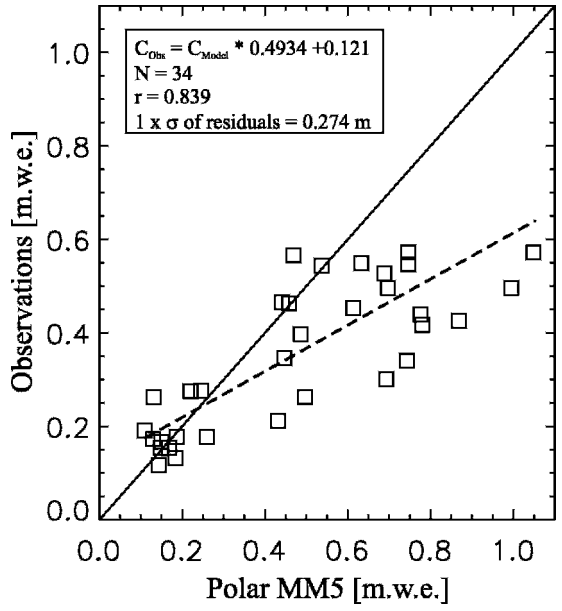

FIG. 4. Comparison between modeled and observed annual (balance year) accumulation rate based on snow pits; locations are shown in Fig. 2.

Furthermore, model errors exhibit a decrease in error magnitude with elevation simply because the accumulation rates decrease with elevation and distance from the coast. Therefore, we incorporate the residual errors with elevation as an explanatory independent variable to derive an empirical (cubic) function to represent the elevation profile of surface mass uncertainty. Owing to spatial variations in surface mass balance magnitude (i.e., north–south, east–west), we create a normalized (fractional) uncertainty model to apply over the whole ice sheet to determine total ice sheet surface mass balance uncertainty and uncertainty related to its temporal changes. The normalized uncertainty model accounts for changing equilibrium line altitude around the ice sheet. Implications of this simple uncertainty model are discussed in the conclusions.

d. Trend analysis

Temporal variability in the 17-yr model output is used to assess the spatial changes in surface mass balance parameters. We test model skill in reproducing temporal variability. The results suggest that Polar MM5 state variables (temperature, pressure, wind speed/direction, humidity, and precipitation) and the atmospheric analyses that drive it, that is, the ECMWF operational analyses, are characterized by usefully high correlation coefficients ($r > 0.8$, in most cases). Thus, Polar MM5 seems to reliably reproduce interannual variability associated with trends. Temporal linear regression for each model grid point establishes a temporal gradient (e.g., mm yr^{-1}) in the case of accumulation. To estimate total ice sheet mass changes (in km^3) water equivalent units (equivalent to Gt), we multiply the temporal gradient by time, yielding the change in the variable over the time period in the regression. We then integrate this change over the whole ice sheet domain, accounting for the grid cell area. For regions with little temporal correlation, that is, slope near zero, there is a small temporal gradient. Therefore, errors in total ice sheet mass change integration measured by low temporal correlation grid cells are negligible. We attribute statistical significance using the $1-p$ probability statistic, for example, a $1-p$ value of 0.91 suggests a 91% probability that the regression slope is statistically significant).

6. Results

a. Accumulation rates

Whole ice sheet mass flux results suggest that 15% of the total solid plus liquid precipitation (641 $km^3\ yr^{-1}$) is lost by surface sublimation/evaporation (64 $km^3\ yr^{-1}$) and blowing snow sublimation (34 $km^3\ yr^{-1}$) (Table 3).

TABLE 3. Annual surface mass balance and related components and their change 1988–2004. Units are km^3 w. e. with Gt units. Variables P, P_{liquid}, E, Q_S, C, M, R, and B are defined in section 3: r is the correlation coefficient of the mass balance term vs year.

Year	P_{solid}	P_{liquid}	E	Q_S	C	M	R	B	AAR
1988	610	19	70	37	522	413	309	213	0.83
1989	583	24	67	32	508	495	362	146	0.80
1990	620	19	69	31	538	568	446	92	0.76
1991	634	19	63	33	556	494	364	192	0.80
1992	622	11	64	36	533	282	201	331	0.87
1993	591	25	56	32	528	488	377	150	0.78
1994	556	22	60	36	482	424	320	162	0.80
1995	561	23	63	36	484	472	364	120	0.79
1996	657	22	58	40	580	391	289	292	0.86
1997	638	25	67	36	560	500	376	184	0.81
1998	590	26	71	36	509	607	483	26	0.75
1999	608	23	62	33	536	472	348	188	0.81
2000	610	35	62	34	549	509	381	169	0.80
2001	657	24	60	28	593	498	379	215	0.81
2002	646	27	64	31	579	613	447	132	0.76
2003	673	37	65	32	613	627	483	130	0.77
2004	629	29	72	33	554	541	407	147	0.79
Mean	**617**	**24**	**64**	**34**	**543**	**494**	**373**	**170**	**0.80**
Min	556	11	56	28	482	282	201	26	0.75
Max	673	37	72	40	613	627	483	331	0.87
Range	117	26	16	12	131	345	282	305	0.12
Linear change	**50**	**14**	**0**	**3**	**68**	**146**	**112**	**−43**	**−0.03**
r	0.54	0.70	0.02	0.27	0.56	0.50	0.47	−0.18	−0.29

Cogley (2004) derived an annual total ice sheet mass accumulation rate of 506 km^3 yr^{-1} with a ± 39 km^3 yr^{-1} "two standard deviation error" uncertainty based on interpolation of ice core accumulation rates representative of a recent 30-yr period (roughly the 1960s–90s). Our result for 17-yr mean accumulation is 543 km^3 yr^{-1} (Table 3), nearly above the apparent 95% confidence observational uncertainty implied by Cogley (2004, i.e., 545 km^3 yr^{-1}). Year 2003 accumulation (613 km^3 yr^{-1}) is extreme (Krabill et al. 2004; Box et al. 2005; Nghiem et al. 2005). However, 40% of the 1988–2004 modeled annual accumulation rates exceed the upper limit of two standard errors of Cogley (2004), more than half of these since 2000 when rapid warming is evident.

The spatial distribution of the 17-yr average accumulation rate (Fig. 5a) exhibits widely recognized spatial patterns found from interpolation of ice core and snow pit data (e.g., Ohmura et al. 1999; Calanca et al. 2000; Cogley 2004). We estimate a calibrated maximum accumulation in the southeastern sector of 1454 mm yr^{-1} in the vicinity of 64.8°N, 40.7°W; 390-m elevation. The earlier (1991–2000) uncalibrated estimate was 1826 mm yr^{-1} at the same grid location (Box et al. 2004). A calibrated minimum value of 174 mm yr^{-1} is simulated in the vicinity of 77.7°N, 38.1°W; 2432 m. The value is larger than derived from earlier ice-core-based estimates and possibly reflects recent accumulation rate increases.

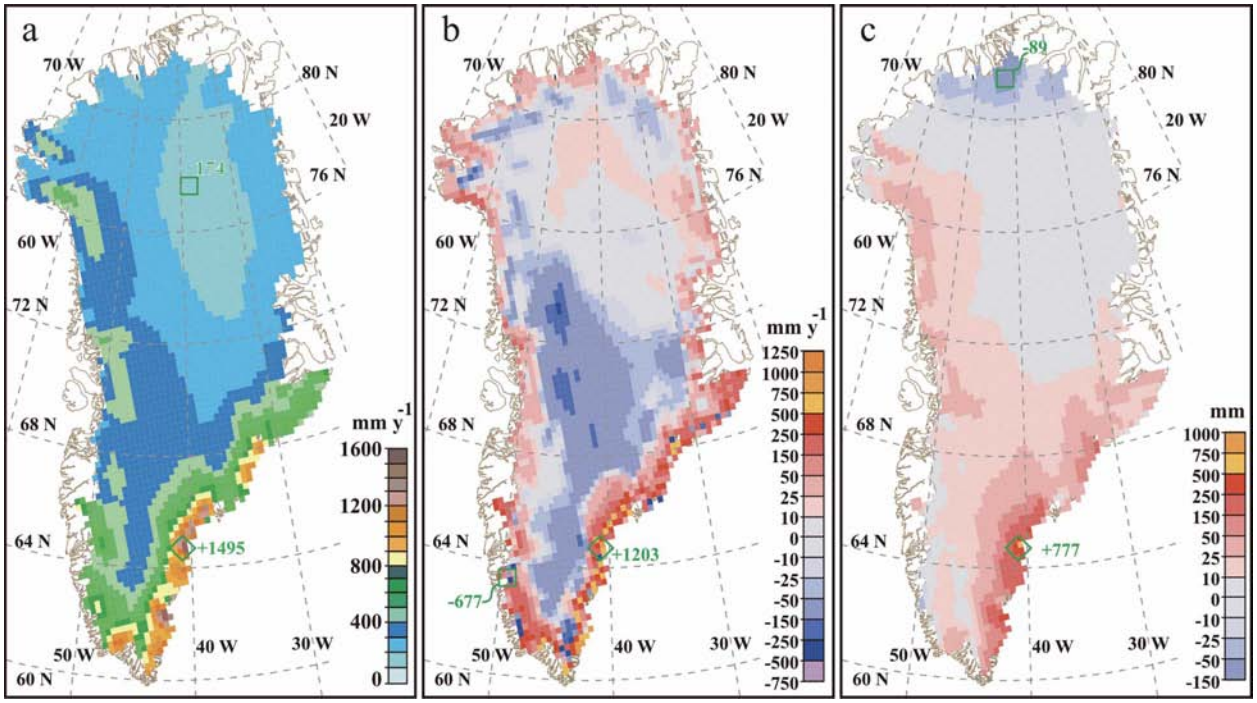

FIG. 5. (a) Average annual accumulation rate (1988–2004), (b) difference with Calanca et al. (2000), and (c) the 17-yr linear regression accumulation change. Minima (squares) and maxima (diamonds) are indicated.

The difference (model minus observation) between the (1988–2004) Polar MM5 accumulation result and a distance-weighted 12-km search interpolation of the ~5 km Calanca et al. (2000) climatology data (Fig. 5b) suggests two likely sources of error. The first is that Polar MM5 modeled orographic precipitation is too high in the region of steepest slopes near the coast. Apparently as a consequence of precipitation falling out prematurely nearer the ice margin, central Greenland precipitation rates seem too low. The second likely possibility for the near-coastal disparity may be the fact that no ablation zone accumulation data are available for the observational climatology and therefore interpolation between accumulation zone observations and coastal precipitation gauge data fail to represent high accumulation values in this intermediate zone. In support of the Polar MM5 results, a similar comparison between RCM and observed Antarctic ice sheet surface mass balance (van de Berg and van den Broeke 2005, manuscript submitted to *J. Geophys. Res.*) showed the same bias pattern. In this case, the elevation gradient in observed accumulation rate suggests that the model orographic overestimation is not as large as the interpolation of observations across areas of high accumulation rate implies. Therefore, the apparent positive bias in near-coastal accumulation rates from this study seems at least exaggerated. However, the inland negative bias is not explained by interpolation shortcomings nor recent accumulation increases. It seems clear that more accumulation observations are needed for high accumulation areas in southeast Greenland. In the case of whole ice sheet accumulation assessments, the model minus observed accumulation results in some cancellation of errors. Discrepancies in the "ice mask," that is, classification of ice/land/ocean land surface type at the ice margin yielded problematic cases when either the Calanca et al. (2000) grid or the Polar MM5 values were considered to be nonice, result in extremely large errors (i.e., 1203 mm yr^{-1}; Fig. 5b). Including all grid cells suggests an overall larger model result (54 km^3), consistent with recent accumulation increases, but inconclusive for overall accuracy assessment owing to different time periods represented by the two methods.

Integrated over the ice sheet, the 17-yr accumulation rate trends are positive, that is, 68 km^3 (Table 3). An increase of 777 mm (46 mm yr^{-1}) occurs near the southeastern accumulation maximum (Fig. 5c). However, the accumulation trend is not statistically significant anywhere in the model domain above the 85% confidence level, owing to an abrupt increase in 2002–03 modeled precipitation. The trend in the southeast is strongly influenced by a persistent atmospheric anomaly (described below) lasting from September 2002 to April 2003 (Box et al. 2005; Nghiem et al. 2005). Year 2004 precipitation rates are more normal for this 17-yr sample. The overall ice sheet positive trend remains, however, even when 2002 and 2003 are excluded from the analysis, implying that increasing accumulation is occurring over the longer period. Results based on the 40-Yr ECMWF Re-Analysis (ERA-40) also suggest increasing precipitation over this region over the longer (1958–2002) time frame (Hanna et al. 2005). Annual modeled precipitation (1991–2001) has a noteworthy correlation ($r > 0.7$) with station records (Cappelen 2003) in the southeast and in western Greenland.

An overall increase in temperature, concentrated along the west and southeast ice sheet margins and along the topographic divide (Box 2005) has led to an increase in the amount of liquid precipitation. Rainfall increases are evident along the whole western and southeastern margins, up to elevations of roughly 1000 m. Along the extreme southwest margin, rainfall constitutes ~60% of the total precipitation according to our model. Increasing rain rates increase the fraction of total precipitation that is liquid. Here, rain fraction increases of 30% are typical in the RCM simulation, limited to a narrow margin in areas of warming trends, that is, along the western slope, especially near 75°N and over the Sukkertoppen ice cap in western Greenland. Elsewhere along the western margin, rain fraction increases of less than 10%–15% are typical. Increases in liquid water supply have implications for liquid water lubrication of ice sheet flow, as suggested by Zwally et al. (2002).

Accumulation changes were negative and relatively small along the east and northeast and coincide with decreasing temperatures. Although small compared with the southern ice sheet, northern regional accumulation decreases may still be significant owing to lesser accumulation rates and surface mass balance over the northern ice sheet region.

b. The accumulation anomaly of 2002–03

September 2002–April 2003 was characterized by anomalously high sea level pressure (SLP) over the Norwegian Sea and relatively low SLP south of the southern tip of Greenland (Fig. 6a), compared to the 30-yr mean from 1972–2002. This relatively long-duration pattern produced the tendency for anomalous southeasterly mean geostrophic flow favoring increased advection and precipitation over the southeastern Greenland ice sheet slope (Fig. 6b). Accumulation rates during this episode were roughly double the long-term mean for any previous September to April (9 month) period in the National Centers for Environmental Prediction (NCEP)–NCAR reanalysis (NNR) data

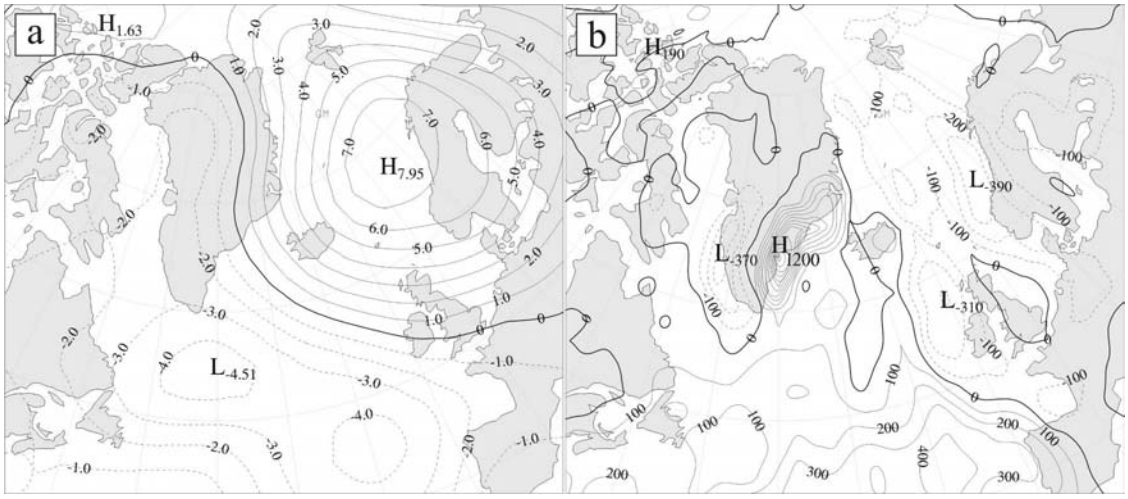

FIG. 6. (a) Mean sea level pressure departures, September 2002–April 2003, compared to a 1972–2002 normal are derived from NNR data. Units are hPa. (b) The accompanying precipitation anomaly (September 2002–April 2003) from the 30-yr average. Units are mm (water equivalent).

(Kalnay et al. 1996) that span 1947–2003. A precipitation shadow effect is evident along the southwest slope (Fig. 6b). This event is noteworthy because it contributes to the positive accumulation trend suggested by the 1988–2004 Polar MM5 result and the precipitation shadow effects contribute to a negative albedo anomaly that amplify warming-related melt increases (Box et al. 2005).

Using SLP data from grid points on the Norwegian Sea pressure anomaly center, and that south of Greenland, permits evaluation of the frequency of previous events of a similar character. The 12-hPa SLP difference between the two centers (Fig. 6a) is unprecedented in the NNR record spanning 1948–2003. Similar, but not as large, maximum differences of 6–8 hPa occur in the winters of 1954, 1960, and 1985 (winter is defined as January and February of the year stated and December of the previous year). Use of a longer (1900–2003) historic pressure record (Trenberth and Paolino 1980) identifies two similar events, in the 8–10-hPa range, occurring in 1929 and 1942. It should be noted that the SLP pattern in Fig. 6a is not characteristic of either mode of the North Atlantic Oscillation.

c. Water vapor fluxes

The 17-yr changes in surface water vapor flux are characterized by increased net losses along the western and southeastern ice sheet margin (Fig. 7a), by as much as 1346 mm (i.e., 79 mm yr^{-1}) in addition to the normal water vapor loss, at 69°N on the western slope. An additional 17-yr loss of 702 mm is simulated at the site of maximum annual warming (6.7 K) in the northwest near 75°N. Above the ELA, the change in evaporation is overall negative, implying more net water vapor deposition. Increased condensation/deposition, or less evaporation/sublimation by up to 41 mm, is simulated along the eastern ice sheet slope. The overall ice sheet surface mass change from surface water vapor flux changes is zero (Table 3), despite coherent spatial trend patterns.

Reapplying the blowing snow sublimation (Q_S) parameterization of Déry and Yau (2001), we estimate the 17-yr change in blowing snow sublimation (Fig. 7b). The pattern suggests increases in blowing snow sublimation are restricted to the southwest slope, while less mass loss by blowing snow sublimation is evident elsewhere. The overall 17-yr change in blowing snow sublimation also is essentially zero (-3 km^3). It is noteworthy that other blowing snow sublimation models (e.g., Bintanja 1998, 2001; Pomeroy and Li 2000) produce differing results. We have not made an exhaustive intercomparison. Nonetheless, we can conclude that precipitation change has likely driven accumulation changes based on our results for surface and blowing snow surface water vapor exchange changes. These spatial patterns of change cancel for the ice sheet overall.

d. Ablation rates

Given widespread increases in temperature (Fig. 1), melt duration (Fig. 8a), and liquid fraction of precipitation associated with warming, statistically significant increases in meltwater production are also evident in the simulation (Fig. 8b). The overall 17-yr change in meltwater production is $+146$ km^3 (Table 3), the largest

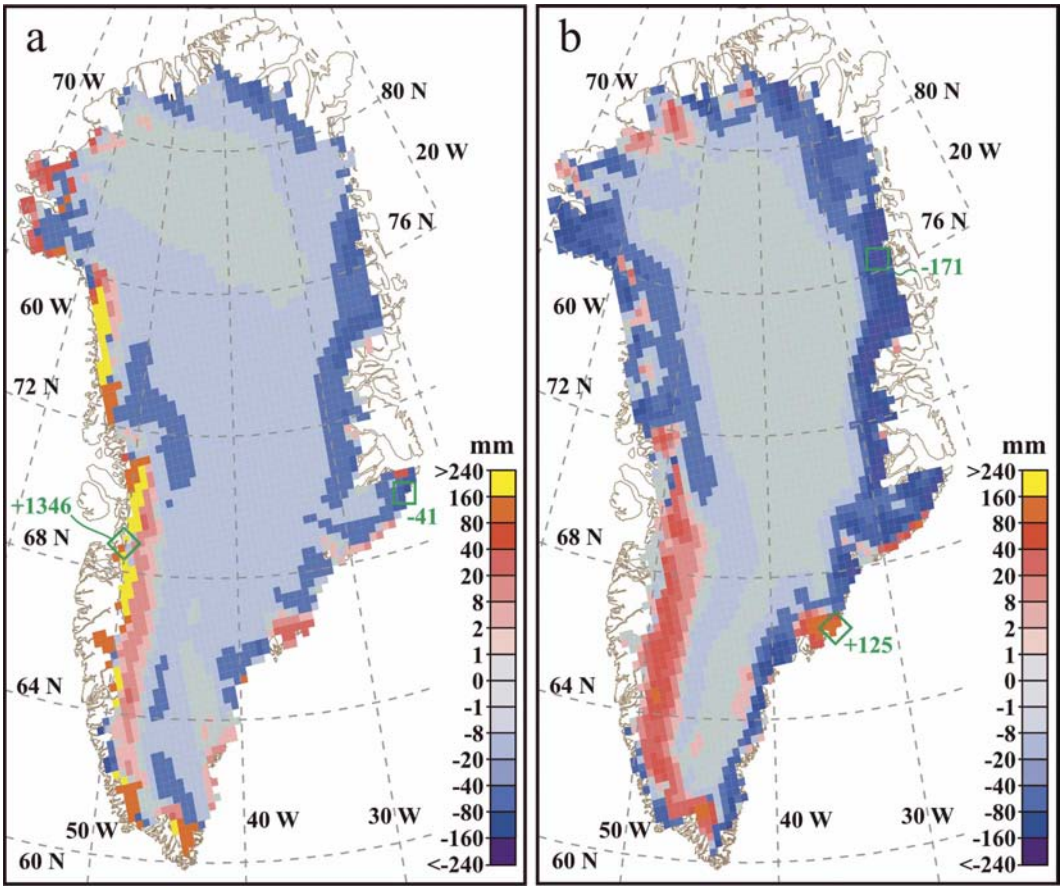

FIG. 7. (a) Annual surface water vapor flux linear change (1988–2004). (b) Blowing snow sublimation change [data based on the parameterization of Déry and Yau (2001)] over the same period. Minima (squares) and maxima (diamonds) are indicated.

change in any of the surface mass budget terms. Minimum meltwater production and runoff are simulated in 1992, the melt year most affected by the Mt. Pinatubo volcanic cooling (Abdalati and Steffen 1997; Box 2002).

The maximum change in meltwater volume production is found in a narrow portion of the southeastern sector (Fig. 8b), where the melt season for that particular 24 km × 24 km area has undergone a 2-month increase melt duration from being an area of essentially no melting. At this extreme, and localized site, the meltwater production has increased by 11 m w.e. over the 17-yr period considered, or 0.65 m yr^{-1}.

e. Ablation changes associated with albedo variability

Owing to the fact that we have two contiguous, yet inhomogeneous, albedo datasets, we present the results for each sensor separately. Figures 9a,b illustrate the melt season average albedo spatial distribution. High albedo is observed at sites with little or no melting, that is, the "dry snow zone." Near the ice margin, albedo values reach their minimum owing to the presence of liquid water, snow/ice grain growth, and dust (e.g., Konzelmann 1994). There are noteworthy differences between the AVHRR- and MODIS-derived albedos. While the inhomogeneity between the two sensors does not allow us to make definitive conclusions about overall 17-yr albedo changes, we observe a similar overall pattern. Comparison of the two albedo "climatologies" suggests a general albedo reduction for the dry snow zone and limited ablation zone areas (e.g., the southwest).

Figures 9c,d illustrate the albedo change over the respective AVHRR and MODIS datasets used in our surface mass balance model. During the earlier AVHRR period, the spatial pattern of albedo change is inconsistent, exhibiting higher spatial variability than temperature and accumulation rate trends suggest. Al-

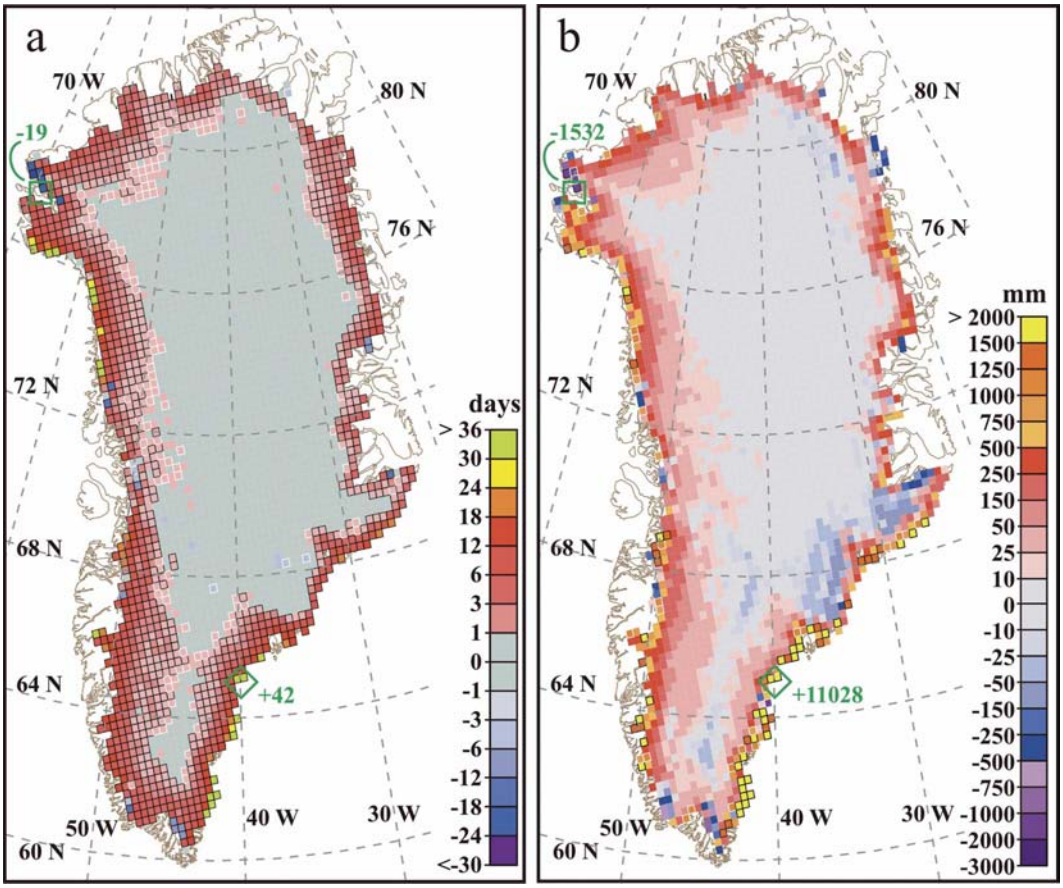

FIG. 8. (a) Change in the days of melting over the 1988–2004 period. (b) Change in meltwater production over the same period. Minima (squares) and maxima (diamonds) are indicated. Statistical significance above the 85% (95%) confidence level is indicated by white (black) outlined grid cells, respectively.

bedo anomalies coincide with temperature change patterns but, again, inconsistency is noticeable. The later 5-yr MODIS change pattern is more consistent and suggests albedo reductions that we would expect during this period of general warming.

In a sensitivity experiment, assuming areas where the albedo is 0.7 or lower are melting, the absorbed solar energy changes for the AVHRR period (1988–99) suggest a 3×10^{21} J decrease in absorbed solar energy for the 1 May–31 August period, corresponding to a solid to liquid water conversion reduction by 11 km^3. This result is small compared to the total mean meltwater production (Table 3) and is complicated by the high degree of spatial variability in albedo change (Fig. 9c). Albedo change over the MODIS period (2000–04) suggests a 16×10^{21} J increase in absorbed solar energy corresponding to a 51 km^3 increase in meltwater production. This result is more consistent, not only spatially, but is consistent with increasing temperatures over this 5-yr period.

Combining the AVHRR and MODIS records into an albedo change map reveals that instrument inhomogeneity masks a reasonable signal. The pattern has a strong latitude gradient, suggesting a systematic error in some part of the angular reflectance modeling, for example, errors in the bidirectional reflectance model and/or sensor scan angle bias. Furthermore, we have become aware of AVHRR geolocation errors that have proven impossible thus far to remove, even using sophisticated image correlation and warping techniques. The 17-yr albedo change suggests melt reductions in areas where we know temperatures have increased in summer. Still, it is clear that data inhomogeneity between the AVHRR and MODIS series do not yet allow them to be used reliably together. As is evident from the modeled surface mass balance changes, albedo errors are less important than expected. In the following, it becomes clear that melt duration and intensity increases have resulted in a large (30%) meltwater production increase (Table 3) owing to strong increases in

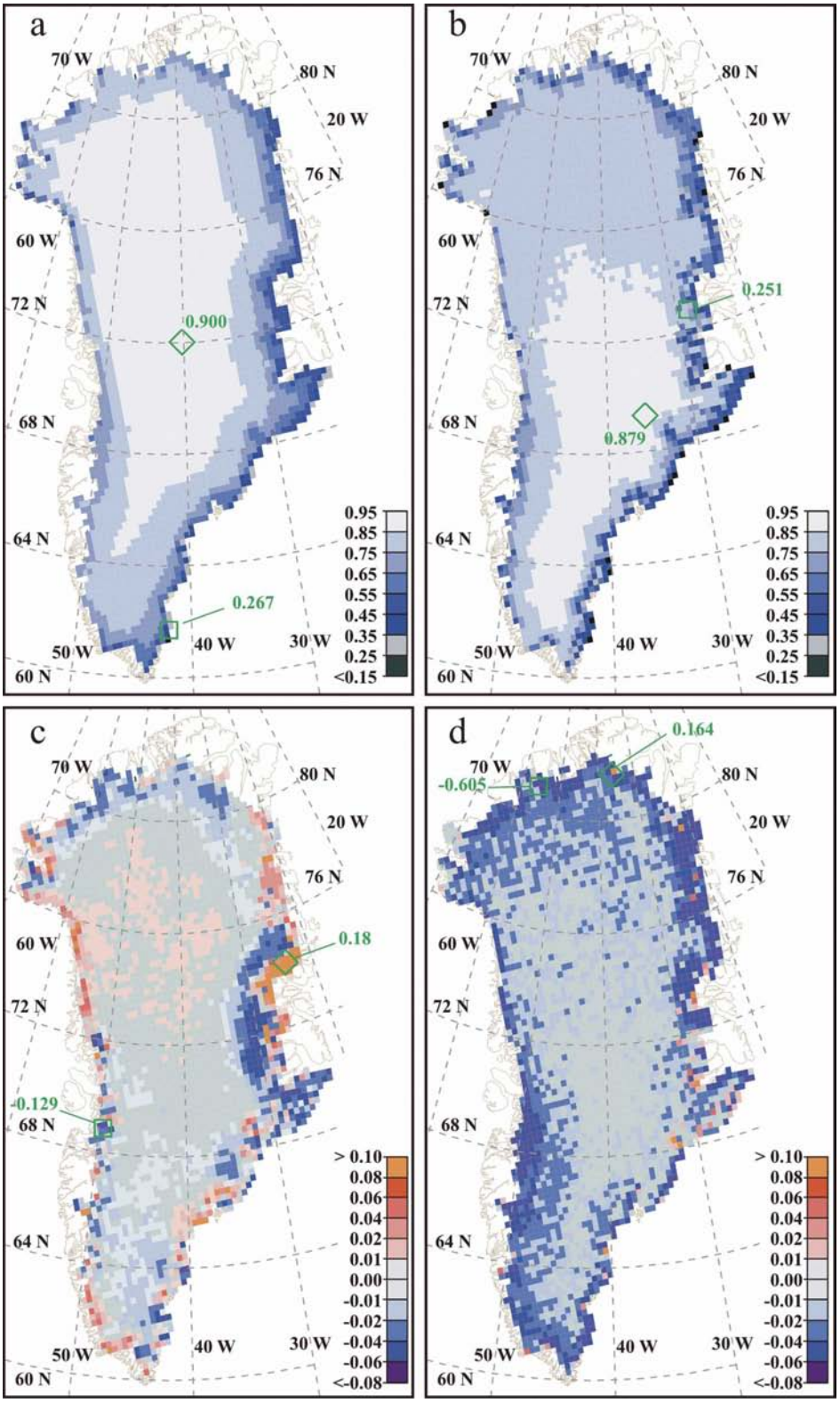

FIG. 9. (a) AVHRR-derived albedo over the 1988–99 (1 May–31 August) period and (b) MODIS-derived albedo over the 2000–04 (1 May–31 August) period. (c) AVHRR-derived albedo change for the 1988–99 (1 May–31 August) period and (d) MODIS-derived albedo change for the 2000–04 (1 May–31 August) period.

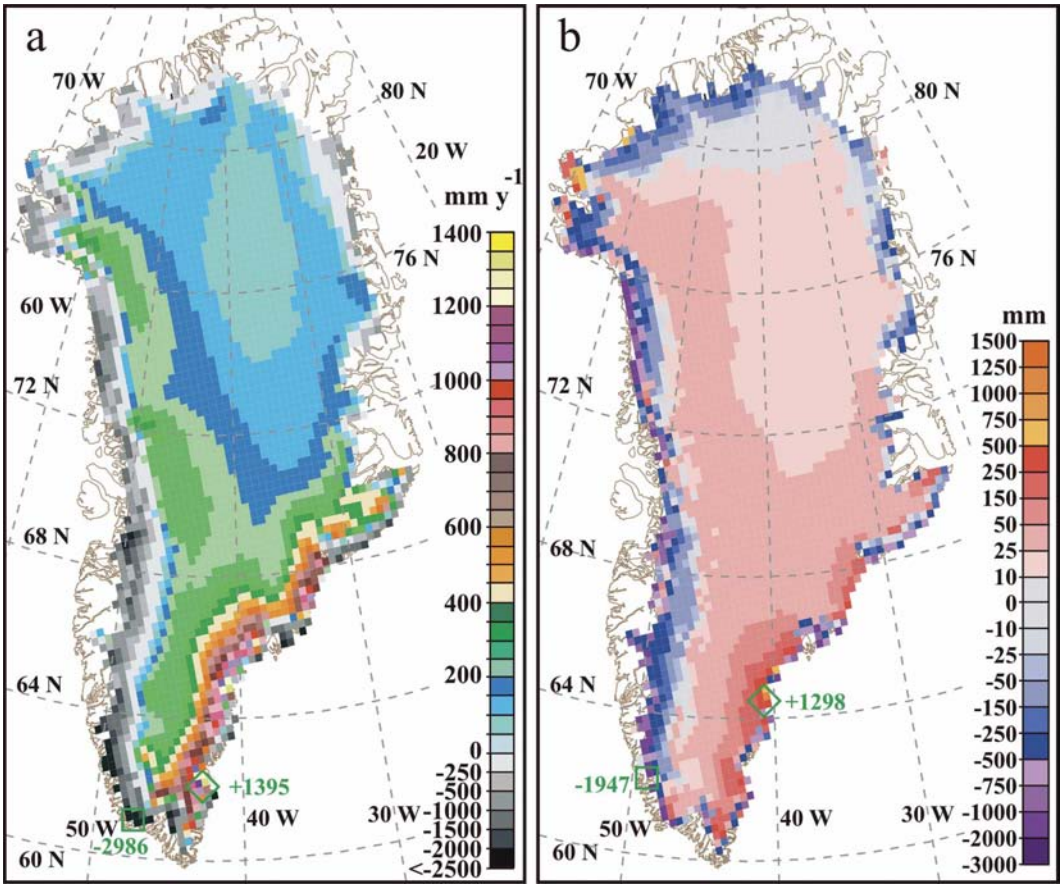

FIG. 10. (a) Average annual surface mass balance (1988–2004) and (b) its 17-yr linear regression change. Minima (squares) and maxima (diamonds) are indicated.

surface temperature, despite inconsistent 17-yr albedo data assimilation trends.

f. Surface mass balance

The 17-yr average surface mass balance estimates from this work (170 $km^3\ yr^{-1}$: Table 3) is 32% less than in Hanna et al. (2002), who suggest the true value is likely smaller. The 17-yr range is almost twice the magnitude, suggesting large interannual fluctuations. A small negative surface mass balance trend is evident from our simulations (Table 3), but not statistically significant. The spatial distribution of the 17-yr mean surface mass balance, calibrated to snow pits and ablation stake data (Fig. 10a), has noteworthy differences from Box et al. (2004). The ablation zone is larger in area owing to larger ablation rate estimates and an increasing ablation trend since 2000. The ELA appears to have increased in altitude, a model result consistent with an observed increasing trend in ice loss at Swiss Camp (situated near the ELA). The ratio of the accumulation zone area to the whole glaciated area; that is, the accumulation area ratio (AAR) has decreased 3% according to our results (Table 3). The combined effect of temperature and precipitation trends over the 17-yr lead to increased rates of ablation and increased accumulation (Fig. 10b). The net effect of these competing factors demonstrates that the overall (total ice sheet) surface mass balance change is relatively small (−2.5 $km^{-3}\ yr^{-1}$). This result is consistent with global climate model estimates (Wild et al. 2003) that predict precipitation increases to somewhat offset the negative mass balance tendencies of warming. Despite this, the Polar MM5 interannual variability does not suggests a significant correlation of temperature and precipitation anomalies.

Although our runoff estimate is larger than all eight estimates compiled by Church et al. (2001), our estimate is only 8% larger than Ohmura et al. (1999) and seems reasonable given recent warming not included in the earlier studies.

A pattern of steepening elevation profiles of net balance has also been observed over many smaller glaciers

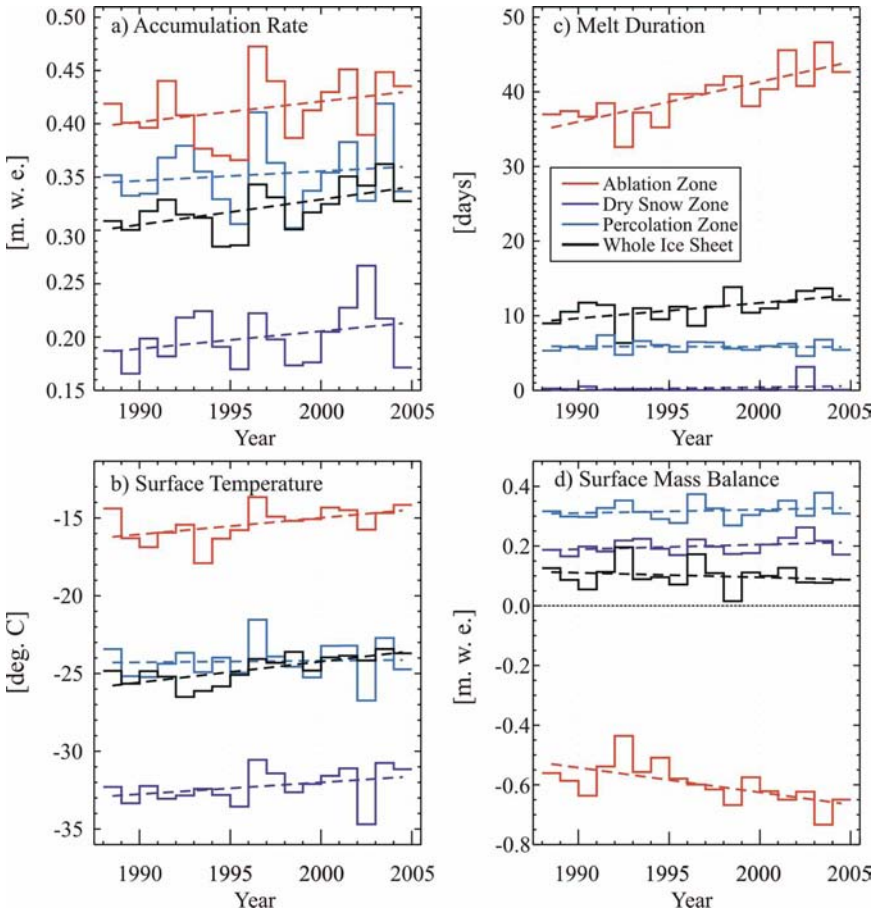

FIG. 11. Time variation of Greenland ice sheet surface mass balance and related quantities averaged over different zones. Trend lines are shown for each zone as dashed lines.

of the Northern Hemisphere (Dyurgerov and Dwyer 2001). The continued peripheral thinning observed by repeat laser altimetry (Krabill et al. 2004) can be at least partially attributed to the trends identified here. Notwithstanding, runoff rates have increased 30% and would suggest a positive contribution to increased ice dynamical flow via the effect measured by Zwally et al. (2002).

g. *Temporal variability*

Mass budget changes are evident in the time series of surface mass balance and related terms (Figs. 11a–d) for the whole ice sheet and for facies zones. The most dramatic changes occur in the ablation zone. The relatively dampened accumulation zone and whole ice sheet signals reflect the larger area occupied by the percolation and dry snow zones. The 17-yr mean AAR was 80% (Table 3). Nonetheless, increases in accumulation rate, surface temperature, and melt duration are evident for the ice sheet as a whole.

The 1996 positive accumulation anomaly (McConnell et al. 2001) is also expressed most clearly in the ablation zone, while the 2002 positive accumulation anomaly is best expressed in the dry snow zone. The 2003 part of the September 2002–April 2003 positive accumulation anomaly (Box et al. 2005; Nghiem et al. 2005) is evident in the percolation zone. There is an overall increasing trend in melt season duration, increasing 10 days on average in the ablation zone, with the expression of the 2002 record melt extent (Steffen et al. 2004; Nghiem et al. 2005) in the dry snow zone. The surface mass balance was nearly negative in 1998 (26 $km^3\ yr^{-1}$), consistent with Hanna et al. (2002), suggesting a strong negative mass balance for the ice sheet as a whole, given that iceberg discharge and basal melting would represent relatively large negative mass budget terms, approximately 239 and 32 $km^3\ yr^{-1}$, respectively, based on a Reeh et al. (1999) ice sheet equilibrium condition. It is therefore likely that, given melt-induced flow acceleration (Zwally et al. 2002), the iceberg discharge term would be much larger than the surface mass balance.

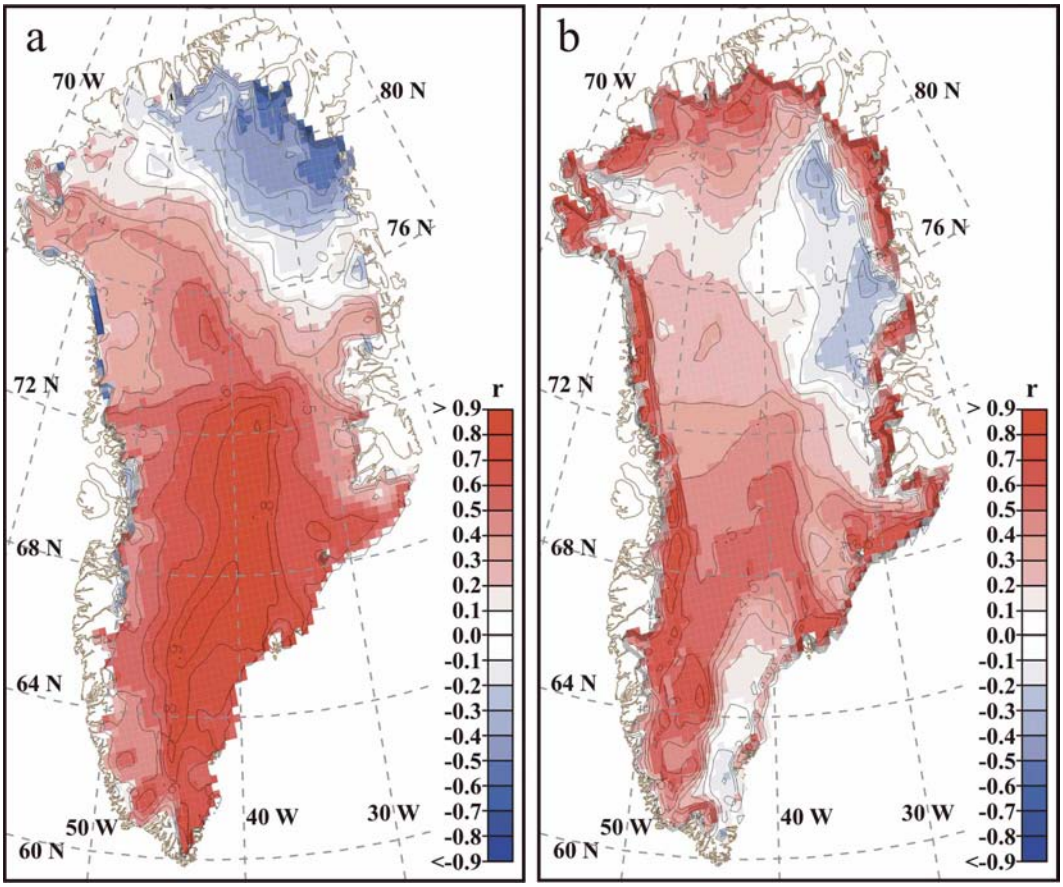

FIG. 12. (a) Spatial pattern of accumulation variability vs total ice sheet accumulation variability (i.e., spatial autocorrelation). (b) Same as (a) but for surface mass balance.

The 1998 ice sheet mass balance would therefore have been at least -200 km^3.

Figure 11 illustrates the counteracting mass changes between the increasingly negative surface mass balance of the ablation zone and the increasingly positive surface mass balance of the accumulation zone (percolation and dry snow zones), for an overall small, but negative, surface mass balance trend during this period of warming (Fig. 1).

h. Spatiotemporal sensitivity

Correlation between time series of the total ice sheet surface mass balance (Table 3) with that at each grid location, that is, spatial autocorrelation, shows where regional variability best captures that of the whole. Highest correlations with accumulation data occur along the ice divide extending from Summit toward the south (Fig. 12a). Maximum autocorrelation occurs near Saddle, presumably where temporal variability represents accumulation from storms impinging up both east and west slopes, that is, from the Denmark and Davis Straits, respectively. This location seems best for an ice core reconstruction of ice sheet mass balance variations (e.g., Zweck and Huybrechts 2005). Zero to negative correlations in the northeast suggest a decoupling of the total ice sheet net accumulation variability with this sector, where a Greenland Sea/Fram Strait climate regime apparently creates an isolated regional variability pattern.

Highest autocorrelation of total ice sheet surface mass balance occurs in the ablation zone and to a lesser extent along the central ice divide (Fig. 12b). The overall pattern suggests that accumulation variability is of lesser importance than melt variability in influencing the surface mass balance. Because the ablation zone calibration data are averaged into a single multiyear correction function, any temporal correlation is caused by variability contained in the model. The region of low correlation in the southeastern ablation zone corresponds to the area of high anomalous accumulation occurring during 2002–03 (Fig. 7b).

i. Ice sheet mass balance

There is currently no conclusive estimate for whole Greenland ice sheet glacier discharge (D) nor basal melting (M_B) rates. The sum of D and M_B constitutes the remainder of mass loss after runoff and net surface water vapor fluxes (E and Q_S), the latter a relatively small negative term overall (Table 3). Reeh et al. (1999, hereafter R99) estimated these terms for a condition of ice sheet equilibrium with surface mass balance. The R99 accumulation rate (547 $km^3\ yr^{-1}$) is nearly equal to the mean value from this study (543 $km^3\ yr^{-1}$). The R99 runoff, however, is 97 $km^3\ yr^{-1}$ less than the mean value from this study; the difference is attributable to recent (2000–04) warming. The R99 ice sheet mass balance assumption does not, however, account for the melt-induced outlet glacier acceleration observed by Zwally et al. (2002). Therefore, the R99 glacier discharge probably represents a minimum value in the present scenario of increased meltwater supply. Therefore, using the R99 D and M_B provides a conservative baseline to estimate ice sheet mass balance with surface mass budget terms from this study. The R99 glacier discharge (239 $km^3\ yr^{-1}$) and basal melting (32 $km^3\ yr^{-1}$) combined with the mean surface mass balance value from this study (170 $km^3\ yr^{-1}$) suggests an ice sheet mass imbalance over this period of at least -100 $km^3\ yr^{-1}$. This mass loss would contribute at least 10% to the 2.9 mm yr^{-1} global sea level rise observed by satellite altimeters (1993–2004; Leuliette et al. 2004). Considering that R99 does not consider melt-induced acceleration, the Greenland ice sheet was probably the largest single glacial contributor to global sea level rise, contributing at least an equivalent amount as that of Alaskan glaciers (Arendt et al. 2002) and at least 2.7 times that of Patagonian ice fields (Rignot et al. 2003). Antarctic Peninsula warming (Vaughn et al. 2003) and post-Larsen B ice shelf breakup glacier acceleration (Scambos et al. 2004) suggest a possible Antarctic sea level contribution that may be offset by increased snow accumulation (Davis et al. 2005). Therefore, based on this current state of knowledge of global land ice fluctuations, we may expect continued global sea level rise given likely future warming scenarios.

7. Conclusions

Results from a 17-yr simulation (1988–2004) from the Polar MM5 regional climate model reveal coherent spatial patterns of temporal change in surface mass balance components over the Greenland ice sheet during a period of warming. While increasing temperatures have led to an increase in the duration of the melt period of over one month in some areas and a 30% increase in meltwater runoff for the ice sheet as a whole, increases in precipitation mostly offset this negative surface mass balance perturbation. However, increases in meltwater suggest an increase in glacier discharge, given observed meltwater-induced ice sheet flow acceleration. Considering even conservative estimates for glacier discharge and basal melting, it seems very likely that the ice sheet lost at least 100 $km^3\ yr^{-1}$ during this warming period, larger than from any other glacier region on earth.

Despite calibration with independent observations and apparently coherent and systematic increases in the hydrologic cycle throughput associated with warming, the accuracy of our model needs to be improved by roughly a factor of 2 to produce definitive assessments of surface mass budget terms and their temporal changes. One standard deviation of residual error from a calibration set of 135 surface mass "balance-year" point measurements suggests an overall uncertainty of 200 km^3 for any given year, the uncertainty reflecting errors in our model and observations. We conclude, however, that the Greenland ice sheet will, in all likelihood, continue to lose mass in a warming climate for the following reasons: 1) the variability of the total ice sheet surface mass balance has a distinctly higher autocorrelation in the ablation zone (in other words, the variability of the whole is best represented by the ablation zone variability); 2) the change in surface mass balance has been negative (-43 km^3) over this 17-yr period, accompanied by both a 3% reduction in accumulation area ratio and temperature increases in all seasons (besides cooling in the northeast); 3) outlet glaciers have been observed to accelerate rapidly (Joughin et al. 2004) during this period when surface meltwater production increased by 30%; and 4) Zwally et al. (2002) demonstrate ice sheet acceleration during periods of increased surface meltwater production.

Acknowledgments. This work was supported by NASA Grant NNG04GH70G. R. Huff and N. Cullen assisted in Greenland Climate Network maintenance and snow pit data collection. K. Knowles of NSIDC provided assistance working with satellite-derived albedo data. We thank S. J. Marshall and an anonymous reviewer for many constructive comments.

REFERENCES

Abdalati, W., and K. Steffen, 1997: The apparent effect of the Mt. Pinatubo eruptions on the Greenland ice sheet melt conditions. *Geophys. Res. Lett.,* **24,** 1795–1797.

Arendt, A. A., K. A. Echelmeyer, W. D. Harrison, C. S. Lingle, and V. B. Valentine, 2002: Rapid wastage of Alaska glaciers and their contribution to rising sea level. *Science,* **297,** 382–386.

Baldwin, D., and W. J. Emery, 1995: Spacecraft attitude variations of *NOAA-11* inferred from AVHRR imagery. *Int. J. Remote Sens.,* **16,** 531–548.

Benson, C. S., 1962: Stratigraphic studies in the snow and firn of Greenland ice sheet. U.S. Army Cold Regions Research and Engineering Laboratory (CRREL) Research Rep. 70, 93 pp.

Bintanja, R., 1998: The contribution of snowdrift sublimation to the surface mass balance of Antarctica. *Ann. Glaciol.,* **27,** 251–259.

——, 2001: Snowdrift sublimation in a katabatic wind region of the Antarctic ice sheet. *J. Appl. Meteor.,* **40,** 1952–1966.

Box, J. E., 2002: Survey of Greenland instrumental temperature records: 1873-2001. *Int. J. Climatol.,* **22,** 1829–1847.

——, 2005: Greenland [in "State of the Climate in 2004"]. *Bull. Amer. Meteor. Soc.,* **86** (6), 41–94.

——, and A. Rinke, 2003: Evaluation of Greenland ice sheet surface climate in the HIRHAM regional climate model. *J. Climate,* **16,** 1302–1319.

——, D. H. Bromwich, and L.-S. Bai, 2004: Greenland ice sheet surface mass balance for 1991–2000: Application of Polar MM5 mesoscale model and in-situ data. *J. Geophys. Res.,* **109,** D16105, doi:10.1029/2003JD004451.

——, L. Yang, J. Rogers, D. Bromwich, L.-S. Bai, K. Steffen, J. C. Stroeve, and S.-H. Wang, 2005: Extreme precipitation events over Greenland: Consequences to ice sheet mass balance. Preprints, *Eighth Conf. on Polar Meteorology and Oceanography,* San Diego, CA, Amer. Meteor. Soc., CD-ROM, 5.2.

Bromwich, D. H., J. Cassano, T. Klein, G. Heinemann, K. Hines, K. Steffen, and J. E. Box, 2001a: Mesoscale modeling of katabatic winds over Greenland with the Polar MM5. *Mon. Wea. Rev.,* **129,** 2290–2309.

——, Q. S. Chen, L. S. Bai, E. N. Cassano, and Y. Li, 2001b: Modeled precipitation variability over the Greenland Ice Sheet. *J. Geophys. Res.,* **106,** 33 891–33 908.

——, L.-S. Bai, and G. G. Bjarnason, 2005: High-resolution regional climate simulations over Iceland using Polar MM5. *Mon. Wea. Rev.,* **133,** 3527–3547.

Calanca, P., H. Gilgen, S. Ekholm, and A. Ohmura, 2000: Gridded temperature and accumulation distributions for use in cryospheric models. *Ann. Glaciol.,* **31,** 118–120.

Cappelen, J., 2003: World weather records 1991–2000—Denmark, The Faroe Islands and Greenland. Tech. Rep. 03-34, Danish Meteorological Institute, Copenhagen, Denmark, 45 pp.

——, 2004: Yearly mean temperature for selected meteorological stations in Denmark, the Faroe Islands and Greenland: 1873–2003. Tech. Rep. 04-07, Danish Meteorological Institute, Copenhagen, Denmark, 9 pp.

Cassano, J., J. E. Box, D. H. Bromwich, L. Li, and K. Steffen, 2001: Verification of Polar MM5 simulations of Greenland's atmospheric circulation. *J. Geophys. Res.,* **106,** 33 867–33 890.

Church, J. A., J. M. Gregory, P. Huybrechts, M. Kuhn, C. Lambeck, M. T. Nhuan, D. Qin, and P. L. Woodworth, 2001: Changes in sea level. *Climate Change 2001: The Scientific Basis,* J. T. Houghton et al., Eds., Cambridge University Press, 639-694.

Cogley, J. G., 2004: Greenland accumulation: An error model. *J. Geophys. Res.,* **109,** D18101, doi:10.1029/2003JD004449.

Davis, C. H., Y. Li, J. R. McConnell, M. M. Frey, and E. Hanna, 2005: Snowfall-driven growth in east Antarctic Ice Sheet mitigates recent sea-level rise. *Science,* **308,** 1898–1901.

Déry, S. J., and M. K. Yau, 2001: Simulation of blowing snow in the Canadian Arctic using a double-moment model. *Bound.-Layer Meteor.,* **2,** 297–316.

Dethloff, K., and Coauthors, 2002: Recent Greenland accumulation estimated from regional climate model simulations and ice core analysis. *J. Climate,* **15,** 2821–2832.

Dyurgerov, M. B., and J. D. Dwyer, 2001: The steepening of glacier mass balance gradients with northern hemisphere warming. *Z. Gletsch. Glazialgeol.,* **36,** 107–118.

Ekholm, S., 1996: A full coverage, high-resolution topographic model of Greenland computed from a variety of digital elevation data. *J. Geophys. Res.,* **101,** 21 961–21 972.

Greuell, W., B. Denby, R. S. W. van de Wal, and J. Oerlemans, 2001: Ten years of mass-balance measurements along a transect near Kangerlussuaq, Greenland. *J. Glaciol.,* **47,** 157–158.

Hanna, E., P. Huybrechts, and T. Mote, 2002: Surface mass balance of the Greenland ice sheet from climate analysis data and accumulation/runoff models. *Ann. Glaciol.,* **35,** 67–72.

——, ——, I. Janssens, J. Cappelen, K. Steffen, and A. Stephens, 2005: Runoff and mass balance of the Greenland ice sheet: 1958–2003. *J. Geophys. Res.,* **110,** D13108, doi:10.1029/2004JD005641.

Hansen, J., R. Ruedy, J. Glascoe, and M. Sato, 1999: GISS analysis of surface temperature change. *J. Geophys. Res.,* **104,** 30 997–31 022.

Jones, P. D., and M. E. Mann, 2004: Climate over past millennia. *Rev. Geophys.,* **42,** RG2002, doi:10.1029/2003RG000143.

Joughin, I., W. Abdalati, and M. Fahnestock, 2004: Large fluctuations in speed on Greenland's Jakobshavn Isbræ glacier. *Nature,* **432,** 608–610.

Kalnay, E., and Coauthors, 1996: The NCEP/NCAR 40-Year Reanalysis Project. *Bull. Amer. Meteor. Soc.,* **77,** 437–471.

Key, J., C. Fowler, J. Maslanik, T. Haran, T. Scambos, and W. Emery, 2002: The Extended AVHRR Polar Pathfinder (APP-x) Product, v 1.0. Digital Media, Space Science and Engineering Center, University of Wisconsin, Madison, WI.

Kiilsholm, S., J.H. Christensen, K. Dethloff, and A. Rinke, 2003: Net accumulation of the Greenland ice sheet: High resolution modeling of climate changes. *Geophys. Res. Lett.,* **30,** 1485, doi:10.1029/2002GL015742.

Konzelmann, T. M., 1994: Radiation conditions on the Greenland ice sheet, Ph.D. thesis, Zürcher Geographischen Schriften, No. 56, Verlag Geographisches Instutut ETH, Zürich, Switzerland, 122 pp.

Krabill, W., and Coauthors, 2004: Greenland Ice Sheet: Increased coastal thinning. *Geophys. Res. Lett.,* **31,** L24402, doi:10.1029/2004GL021533.

Leuliette, E., R. Nerem, and G. Mitchum, 2004: Calibration of TOPEX/Poseidon and Jason altimeter data to construct a continuous record of mean sea level change. *Mar. Geod.,* **27** (1–2), 79–94.

Liang, S., J. C. Stroeve, and J. E. Box, 2005: Mapping daily snow/ice shortwave broadband albedo from Moderate Resolution Imaging Spectroradiometer (MODIS): The improved direct retrieval algorithm and validation with Greenland in situ measurement. *J. Geophys. Res.,* **110,** D10109, doi:10.1029/2004JD005493.

McConnell, J. R., G. Lamorey, E. Hanna, E. Mosley-Thompson, R. C. Bales, D. Belle-Oudry, and J. D. Kyne, 2001: Annual net snow accumulation over southern Greenland from 1975 to 1998. *J. Geophys. Res.,* **106,** 33 827–33 838.

Nghiem, S. V., K. Steffen, G. Neumann, and R. Huff, 2005: Mapping of ice layer extent and snow accumulation in the percolation zone of the Greenland ice sheet. *J. Geophys. Res.,* **110,** F02017, doi:10.1029/2004JF000234.

Oerlemans, J., and H. F. Vugts, 1993: A meteorological experiment in the melting zone of the Greenland ice sheet. *Bull. Amer. Meteor. Soc.,* **74,** 355–365.

Ohmura, A., P. Calanca, M. Wild, and M. Anklin, 1999: Precipitation, accumulation, and mass balance of the Greenland ice sheet. *Z. Gletsch. Glazialgeol.,* **35,** 1–20.

Pfeffer, W. T., M. F. Meier, and T. H. Illangasekare, 1991: Retention of Greenland runoff by refreezing: Implications for projected future sea-level change. *J. Geophys. Res.,* **96,** 22 117–22 124.

Pomeroy, J. W., and L. Li, 2000: Prairie and Arctic areal snow cover mass balance using a blowing snow model. *J. Geophys. Res.,* **105,** 26 619–26 634.

Rao, C. R. N., and J. Chen, 1995: Inter-satellite calibration linkages for the visible channels of the Advanced Very High Resolution Radiometer on the *NOAA-8, -9,* and *-11*. *Int. J. Remote Sens.,* **16,** 1931–1942.

Reeh, N., C. Mayer, H. Miller, H. H. Thomson, and A. Weidick, 1999: Present and past climate control on fjord glaciations in Greenland: Implications for IRD-deposition in the sea. *Geophys. Res. Lett.,* **26,** 1039–1042.

Rignot, E., A. Rivera, and G. Casassa, 2003: Contribution of the Patagonian Icefields of South America to sea level rise. *Science,* **302,** 434–437.

Scambos, T. A., J. A. Bohlander, C. A. Shuman, and P. Skvarca, 2004: Glacier acceleration and thinning after ice shelf collapse in the Larsen B embayment, Antarctica. *Geophys. Res. Lett.,* **31,** L18402, doi:10.1029/2004GL020670.

Steffen, K., and J. E. Box, 2001: Surface climatology of the Greenland ice sheet: Greenland Climate Network 1995–1999. *J. Geophys. Res.,* **106,** 33 951–33 964.

——, ——, and W. Abdalati, 1996: Greenland climate network: GC-Net. Glaciers, Ice Sheets, and Volcanoes: A Tribute to Mark F. Meier. CRREL Special Rep. 96-27, 98–103.

——, S. V. Nghiem, R. Huff, and G. Neumann, 2004: The melt anomaly of 2002 on the Greenland ice sheet from active and passive microwave satellite observations. *Geophys. Res. Lett.,* **31,** L20402, doi:10.1029/2004GL020444.

Stroeve, J. C., J. E. Box, J. Maslanik, J. Key, and C. Fowler, 2001: Intercomparison between in situ and AVHRR Polar Pathfinder-derived surface albedo over Greenland. *Remote Sens. Environ.,* **75,** 360–374.

——, ——, A. Nolin, S. Liang, C. Schaaf, and F. Gao, 2005: Accuracy assessment of the MODIS 16-day albedo product for snow: Comparisons with Greenland in situ measurements. *Remote Sens. Environ.,* **94,** 46–60.

Trenberth, K. E., and D. A. Paolino Jr., 1980: The Northern Hemisphere sea level pressure data set: Trends, errors and discontinuities. *Mon. Wea. Rev.,* **108,** 855–872.

van den Broeke, M. R., D. van As, C. H. Reijmer, and R. S. W. van de Wal, 2004: Assessing and improving the quality of unattended radiation observations in Antarctica. *J. Atmos. Oceanic Technol.,* **21,** 1417–1432.

van der Veen, C. J., 2002: Polar ice sheets and global sea level: How well can we predict the future? *Global Planet. Change,* **32,** 165–194.

Vaughan, D. G., and Coauthors, 2003: Recent rapid regional climate warming on the Antarctic Peninsula. *Climate Change,* **60,** 243–274.

Wild, M., P. Calanca, S. C. Scherrer, and A. Ohmura, 2003: Effects of polar ice sheets on global sea level in high-resolution greenhouse scenarios. *J. Geophys. Res.,* **108,** 4165, doi:10.1029/2002JD002451.

Zwally, H. J., W. Abdalati, T. Herring, K. Larsen, J. Saba, and K. Steffen, 2002: Surface melt-induced acceleration of Greenland ice-sheet flow. *Science,* **297,** 218–222.

Zweck, C., and P. Huybrechts, 2005: Modeling of the Northern Hemisphere ice sheets during the last glacial cycle and glaciological sensitivity. *J. Geophys. Res.,* **110,** D07103, doi:10.1029/2004JD005489.